



Modeling an ordered nanostructured cathode catalyst layer for proton exchange membrane fuel cells

M.M. Hussain*, D. Song, Z.-S. Liu, Z. Xie

Institute for Fuel Cell Innovation, National Research Council, Vancouver, BC, Canada V6T 1W5

ARTICLE INFO

Article history:

Received 17 August 2010

Received in revised form 6 October 2010

Accepted 7 October 2010

Available online 18 January 2011

Keywords:

Ordered nanostructured CCL

PEM fuel cell

Carbon nanotube (CNT)

Knudsen diffusion

ABSTRACT

A 3D mathematical model of an ordered nanostructured cathode catalyst layer (CCL) has been developed for proton exchange membrane (PEM) fuel cells. In an ordered nanostructured CCL, carbon nanotubes (CNTs) are used as support material for Pt catalyst, upon which a thin layer of proton-conducting polymer (Nafion) is deposited, which are then aligned along the main transport direction (perpendicular to the membrane) of various species. The model considers all the relevant processes in different phases of an ordered nanostructured CCL. In addition, the effect of Knudsen diffusion is accounted in the model. The model can predict not only the performance of an ordered nanostructured CCL at various operating and design conditions but also can predict the distributions of various fields in different phases of an ordered nanostructured CCL. The predicted nanostructured CCL performance with estimated membrane overpotential is validated with measured data found in the literature, and a good agreement is obtained between the model prediction and measured result. Moreover, a parametric study is conducted to investigate the effect of key design parameters on the performance of an ordered nanostructured CCL. In the absence of liquid water, it is found that oxygen diffusion in the pore phase is not the limiting factor for the performance of an ordered nanostructured CCL, owing to its parallel gas pores and high porosity. However, the transport of dissolved oxygen through the Nafion phase has a significant effect on the performance of an ordered nanostructured CCL. Further, it is found that increasing the spacing between CNTs results in a considerable drop in the performance of an ordered nanostructured CCL at the base case conditions considered in the simulation.

© 2011 Elsevier B.V. All rights reserved.

1. Introduction

In spite of significant improvements in the performance of PEM fuel cells over the last decade, cost and durability are still the most critical barriers hindering their commercialization [1,2]. Cost reduction can be realized by more efficient use of materials in the electrodes of PEM fuel cells and economy-of-scale in production [3]. For instance, maximizing the platinum (Pt) catalyst utilization in the catalyst layers (CLs) of PEM fuel cells, results in reducing the Pt loading, which in turn helps in cost savings. On the other hand, durability of PEM fuel cells depends on all of their membrane-electrode-assembly (MEA) components. However, the major contributors to the excessive degradation of stack voltage are the Pt surface area loss due to carbon corrosion and Pt dissolution (aggregation) in CLs [4]. Moreover, of the two CLs, CCL is the source of largest potential loss in PEM fuel cells, owing to sluggish kinetics of oxygen reduction reaction (ORR) and the mass transport limitations due to the formation and transport of liquid water.

The conventional state-of-the-art PEM fuel cell CCL contains catalyst, electron conductor, proton conductor and pores. Typically, carbon black is used as the electron conductor on which 2–3 nm sized Pt catalyst particles are finely dispersed. It is usually mixed with proton conducting polymer like Nafion and a solvent to form an ink. Pores are formed during drying of an ink, after the solid particles reached their maximum packing density [3]. Despite its extensive use, carbon black in the conventional CCL is reported to undergo electrochemical oxidation to surface oxides, and finally to CO₂. Consequently, Pt particle agglomerates are formed resulting in the loss of electrochemical surface area (ECSA) [5–13]. Additionally, the morphology of the conventional CCL studied through high resolution scanning electron microscopy (HR-SEM), reveals that a large portion of the Pt catalyst is located deep inside the agglomerates, and is hardly accessible to reactant oxygen leading to inefficient Pt utilization [3,14,15]. Further, there will be increased mass transfer resistance for the reactant gas to reach to the Pt particles located deep inside the agglomerates, resulting in high concentration overpotential.

In order to overcome the issues associated with conventional CCL, such as carbon corrosion leading to loss of ECSA, low Pt utilization resulting in wastage of expensive Pt, and transport limitations resulting in overall performance loss, considerable efforts have

* Corresponding author.

E-mail addresses: Mohammed.Hussain@nrc-cnrc.gc.ca, hussain.mohammedm@gmail.com (M.M. Hussain).

Nomenclature

A_s	catalyst surface area per unit mass of the catalyst, $\text{m}^2 \text{g}^{-1}$
A_v	reactive surface area per unit volume, $\text{m}^2 \text{m}^{-3}$
c	concentration of the mixture in the pore phase, mole m^{-3}
c_0	oxygen concentration at the GDL/CCL interface, mole m^{-3}
c_{H^+}	fixed charge concentration in the membrane, mole m^{-3}
$c_{\text{O}_2\text{-g}}$	gaseous oxygen concentration in the pore phase, mole m^{-3}
$c_{\text{O}_2\text{-m}}$	dissolved oxygen concentration, mole m^{-3}
$c_{\text{O}_2,\text{ref}}$	reference oxygen concentration, mole m^{-3}
d_p	mean pore diameter of the pore equivalent to spacing between two CNTs, nm
d_{CNTs}	distance or spacing between two CNTs, nm
D_{ij}	ordinary diffusion coefficient, $\text{m}^2 \text{s}^{-1}$
$D_{\text{Kn},i}$	Knudsen diffusion coefficient of species i , $\text{m}^2 \text{s}^{-1}$
$D_{\text{O}_2\text{-m}}$	oxygen diffusion coefficient in the Nafion phase, $\text{cm}^2 \text{s}^{-1}$
φ_{ij}	combined diffusion coefficient, $\text{m}^2 \text{s}^{-1}$
$\varphi_{ij}^{\text{eff}}$	effective combined diffusion coefficient, $\text{m}^2 \text{s}^{-1}$
E_r	thermodynamic reversible cell potential, V
F	Faraday's constant, $96,487 \text{ C mole}^{-1}$
$H_{\text{O}_2\text{-m}}$	Henry's constant for oxygen dissolution in the Nafion film, J mole^{-1}
J_m	protonic current density in the Nafion phase, A m^{-2}
$J_{0,\text{ref}}$	reference exchange current density for ORR, A m^{-2}
k	constant, $3.16 \times 10^{-8} \text{ Pa m}^2 \text{s}^{-1}$
K_E	electrokinetic permeability of the membrane, m^2
K_P	hydraulic permeability of the membrane, m^2
L_{CNT}	length of CNT or CCL thickness, μm
m_{Pt}	catalyst loading per unit area of the cathode, mg cm^{-2}
M_i	molecular weight of species i , kg mol^{-1}
N_i	molar flux of species i in the pore phase, $\text{mole m}^{-2} \text{s}^{-1}$
$N_{\text{O}_2\text{-m}}$	molar flux of dissolved oxygen in the Nafion phase, $\text{mole m}^{-2} \text{s}^{-1}$
p	pressure, Pa
p_{H_2}	partial pressure of hydrogen, atm
p_{O_2}	partial pressure of oxygen, atm
r_{CNT}	radius of CNT, nm
r_b	interface between the pore phase and the Nafion phase
R	universal gas constant, $8.3143 \text{ J mole}^{-1} \text{K}^{-1}$
t_m	membrane thickness, μm
t_{Nafion}	nafion film thickness, nm
T	temperature, K
x	x -direction, m
x_i	mole fraction of species i in the pore phase
y	y -direction, m
w_t	mass fraction of species i in the pore phase
z	z -direction, m
Greek	
α_a	anode charge transfer coefficient
α_c	cathode charge transfer coefficient
Δp_{a-c}	pressure difference between the anode and the cathode, Pa
γ	reaction order for ORR
ε_g	porosity or volume fraction of pore phase

ε_m	volume fraction of Nafion phase
η_{act}	cathode activation overpotential, V
η_{ohm}	cathode ohmic overpotential, V
η_0	applied cathode overpotential at the membrane interface, V
η_m	membrane ohmic overpotential, V
κ	intrinsic proton conductivity of Nafion, S m^{-1}
κ^{eff}	effective proton conductivity in the Nafion phase, S m^{-1}
$\mu_{\text{H}_2\text{O}}$	viscosity of the liquid water, $\text{kg m}^{-1} \text{s}^{-1}$
v_i	molar diffusion volume of species i , $\text{m}^3 \text{mole}^{-1}$
ϕ_m	protonic phase potential in the Nafion phase, V
ϕ_s	electronic phase potential in the electron-conducting phase (CNT), V

been dedicated to develop novel catalyst support material for CCL, and the resulting CCL is often referred to as ordered nanostructured or oriented CCL structure [3,4,9,16–32]. In an ordered nanostructured CCL, carbon nanotubes (CNTs) are being used as support material for Pt catalyst owing to their unique features, which include superior mechanical and electrical properties, high aspect ratio and enhanced mass transport capability [16,18,19,33–38]. On the surface of these CNTs, also referred to as electron conductors, Pt particles of approximately 2 nm are finely dispersed. A thin layer of Nafion is then deposited on the Pt-coated CNTs and aligned along the main transport direction (perpendicular to the membrane) of electron, proton and reactant gas to form an ordered or oriented nanostructured CCL.

Generally, it is believed that an oriented nanostructured CCL offers much improved performance than a non-oriented or disordered nanostructured CCL structure because of its following salient features. First, the inherent advantage of an oriented nanostructured CCL, resulting in straight pores, would enhance the transport of oxygen. Second, the Pt particles are located at the interface of the electron conductor (CNTs) and the proton conductor (Nafion) would result in better Pt utilization in an oriented nanostructured CCL. Third, the electronic conductivity of CNTs is much higher along the tubes than across the tubes; as a result, there is negligible loss in potential when electrons transfer along the tubes [39,40]. Fourth, an oriented nanostructured CCL may exhibit superhydrophobicity, which can facilitate greater water removal within the CCL, thereby improving mass transport [18].

Mathematical modeling is an essential tool in understanding the processes occurring in different phases of an oriented nanostructured CCL and helps in gaining insights about the processes influencing the CCL performance. In the recent past, there were few attempts to model an ordered nanostructured CCL. Du et al. [41,42] were few of the earliest researchers to model an ordered nanostructured CCL having straight pores. Later, Chisaka and Daiguji [43] also modeled an ordered nanostructured CCL having triangular orientation of CNTs. These models [41–43] were 1D models and considered mostly the radial diffusion of oxygen through the Nafion film. Moreover, Chisaka and Daiguji [43] did not consider the axial gradient of oxygen concentration induced along the pores. More recently, Rao and Xing [44] developed a 2D model for an ordered nanostructured CCL having square orientation of CNTs. They assumed a thick Nafion film (1 μm) on the surface of CNTs, which is inconsistent with the reported values for an ordered nanostructured CCL and also neglected the proton transport in the Nafion film. Further, none of the models [41–44] were validated with the measured data available in the literature.

The objective of the present study is to develop a 3D model of an ordered nanostructured CCL for PEM fuel cells, which considers

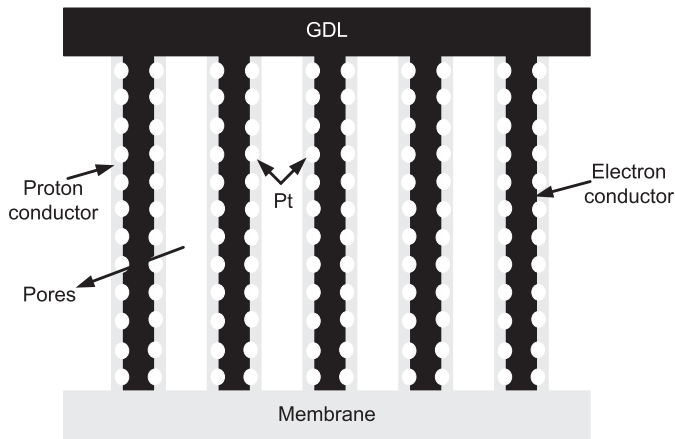


Fig. 1. Schematic representation of an ordered nanostructured CCL.

all the relevant processes in different phases of the nanostructured CCL and simulates its performance using realistic design conditions. Moreover, the other objectives are to validate the predicted nanostructured CCL performance with measured data available in the literature and to assess the effects of key morphological parameters on the performance of an ordered nanostructured CCL.

2. Model formulation

A schematic representation of an ordered nanostructured CCL is shown in Fig. 1. It consists of oriented CNTs, upon which Pt particles are uniformly distributed, and the catalyzed CNTs are finally covered with thin films of Nafion. Oxygen in the multi-component mixture diffuses through the straight pores in between the CNTs, and then diffuses radially through the Nafion film to reach the reaction sites on the surface of CNTs.

In an ordered nanostructured CCL, CNTs can be oriented in any particular fashion. However, in the present study, a square grid orientation of CNTs is considered, which allows using symmetry in the simulation. Fig. 2 illustrates the cross-sectional view of an ordered nanostructured CCL; whereas, Fig. 3 shows the 3D computational domain. The dashed line square in Fig. 2 shows the symmetric cross-sectional portion of an ordered nanostructured CCL in the y-z plane. The computational domain includes the quarter portion of CNT, the Nafion thickness, and half-spacing between two CNTs representing the pore-phase. Moreover, the x-direction represents the length of CNT or CCL thickness. Oxygen in the multi-component mixture diffuses into the CCL through the gas diffusion layer (GDL) on the left boundary (i.e. $x=0$) and protons migrate into the CCL from the membrane side on the right boundary (i.e. $x=L_{CNT}$). Oxygen then dissolves in the Nafion film and is consumed at the reaction boundary (r_{CNT}) along with protons and electrons due to the oxygen reduction reaction (ORR).

The cell is assumed to operate under steady state condition. The temperature and pressure are assumed to be uniform in the CCL. The convective flux is assumed to be negligible when compared to the diffusive flux of species. The multi-component mixture is approximated as ideal gas with negligible viscous, Soret, Dufour and gravity effects. The product water is assumed to be in the gas phase and diffuses out of the CCL sufficiently fast, implying there is no liquid water present in the pore phase of an ordered nanostructured CCL. The proton conductivity in the Nafion phase is assumed to be constant, and due to sufficiently high electronic conductivity of CNTs, the electronic phase potential is assumed to be negligible compared to the protonic phase potential in the CCL. Finally, the Pt catalyst is assumed to be uniformly distributed over the CNT surface, implying ORR occurs at the interface between electron-

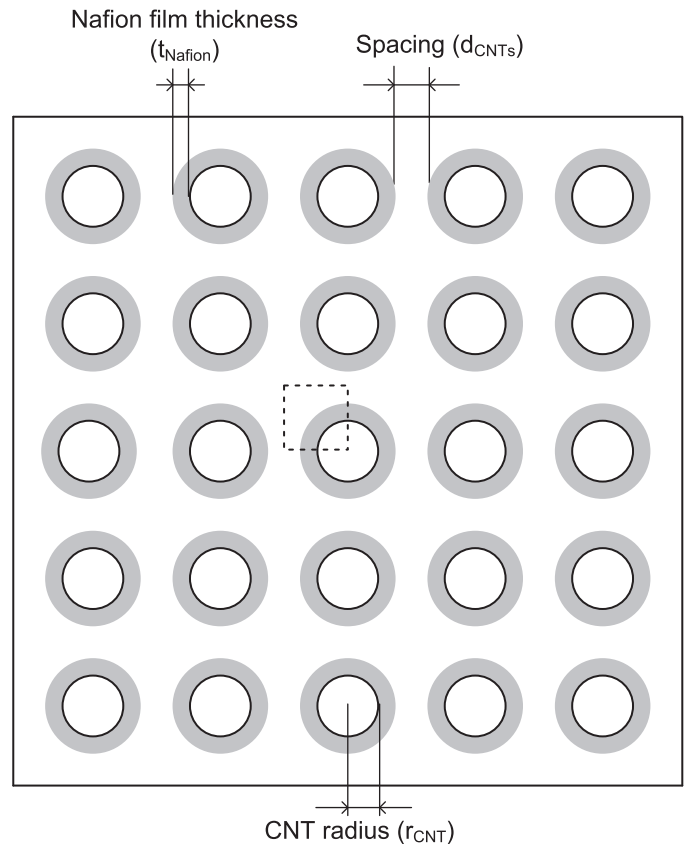


Fig. 2. Cross-sectional view of an ordered nanostructured CCL.

conducting phase (CNT) and proton-conducting phase (Nafion), also referred to as the reaction boundary.

Based on the above stated assumptions, the governing equations for the transport of multi-component mixture in the pore phase, dissolved oxygen transport in the Nafion phase, and proton transport in the Nafion phase are described as follows.

$$\text{Multi-component mixture transport : } \nabla \cdot \vec{N}_i = 0 \tag{1}$$

$$\text{Dissolved oxygen transport : } \nabla \cdot \vec{N}_{O_{2-m}} = 0 \tag{2}$$

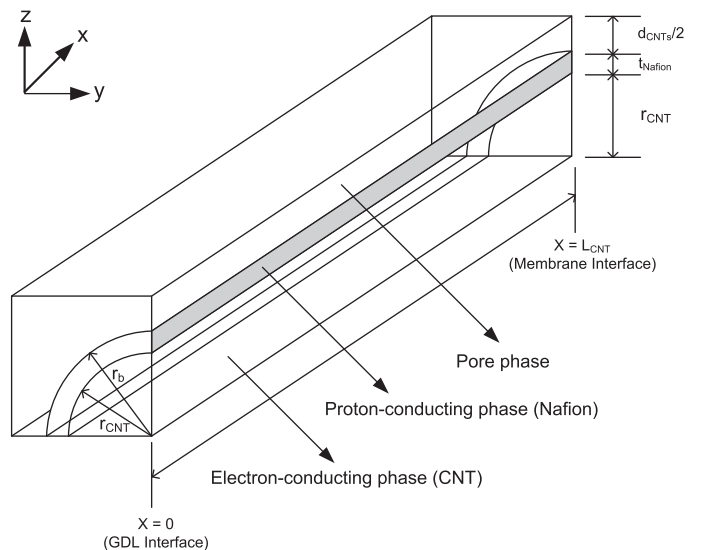


Fig. 3. 3D computational domain of an ordered nanostructured CCL.

$$\text{Proton transport : } \nabla \cdot \vec{J}_m = 0 \quad (3)$$

where \vec{N}_i is the species diffusion flux in the pore phase, $\vec{N}_{O_{2-m}}$ is the diffusion flux of dissolved oxygen in the Nafion phase, and \vec{J}_m is the protonic current density in the Nafion phase.

The diffusion flux in the pore phase can be determined using the modified Stefan–Maxwell equations incorporating Knudsen diffusion for multi-component systems involving n species, expressed as [45]:

$$\nabla x_i = \sum_{j=1}^n \frac{1}{cD_{ij}} (x_i \vec{N}_j - x_j \vec{N}_i) + \frac{\vec{N}_i}{D_{Kn,i}} \quad (4)$$

where c is the concentration of the mixture in the pore phase, D_{ij} is the ordinary diffusion coefficient of species i in j , x_i is the mole fraction of species i in the pore phase, and \vec{N}_i is the diffusion flux of species i in the pore phase, and $D_{Kn,i}$ is the Knudsen diffusion coefficient of species i , which is calculated using the following expression [46–48]:

$$D_{Kn,i} = \frac{1}{3} d_p \sqrt{\frac{8RT}{\pi M_i}} \quad (5)$$

where d_p is the mean pore diameter equivalent to mean distance or spacing between two CNTs (d_{CNTs}) in an ordered nanostructured CCL, R is the universal gas constant in $\text{J mole}^{-1} \text{K}^{-1}$, T is the temperature in K, and M_i is the molecular weight of species i in kg mole^{-1} .

The binary or ordinary diffusion coefficients (D_{ij}) can be calculated using an empirical relation based on the kinetic theory of gases, expressed as [49]:

$$D_{ij} = k \frac{T^{1.75}}{p(v_i^{1/3} + v_j^{1/3})^2} \left[\frac{1}{M_i} + \frac{1}{M_j} \right]^{1/2} \quad (6)$$

where k is a constant with the value $3.16 \times 10^{-8} \text{ Pa m}^2 \text{ s}^{-1}$, T is the temperature in K, p denotes the pressure in Pa, v_i is the molar diffusion volume of species i in $\text{m}^3 \text{ mole}^{-1}$, and M_i is the molecular weight of species i in kg mole^{-1} .

Mathematically, the two terms on the right hand side of Eq. (4) can be combined to obtain the modified Stefan–Maxwell model for multi-component diffusion in the pore phase of an ordered nanostructured CCL, and can be expressed as

$$\nabla x_i = \sum_{j=1}^n \frac{1}{c\phi_{ij}} (x_i \vec{N}_j - x_j \vec{N}_i) \quad (7)$$

where ϕ_{ij} is the combined diffusion coefficient, defined as

$$\phi_{ij} = \left(\frac{D_{ij} D_{Kn,i}}{D_{ij} + D_{Kn,i}} \right) \quad (8)$$

In terms of effective diffusion coefficient, modified Stefan–Maxwell model is expressed as

$$-c \nabla x_i = \sum_{j=1, i}^n \frac{1}{\phi_{ij}^{\text{eff}}} (x_j \vec{N}_i - x_i \vec{N}_j) \quad (9)$$

where ϕ_{ij}^{eff} is the combined effective diffusion coefficient in the pore phase, defined as

$$\phi_{ij}^{\text{eff}} = \varepsilon_g \phi_{ij} \quad (10)$$

where ε_g is pore volume fraction or porosity of an ordered nanostructured CCL. It is worthwhile to note that the effective properties are not corrected for porosity and tortuosity using the Bruggeman correlation. However, in an ordered nanostructured CCL, since the

CNTs are uniformly distributed and form a straight pore network along the axial direction, the effective properties are corrected only with volume fractions of pore or Nafion.

Expressing the dissolved oxygen flux and protonic current density in the Nafion phase in terms of dissolved oxygen concentration and protonic phase potential, respectively, Eqs. (2) and (3) become

$$\text{Dissolved oxygen transport : } \nabla \cdot (D_{O_{2-m}} c_{O_{2-m}}) = 0 \quad (11)$$

$$\text{Proton transport : } \nabla \cdot (\kappa^{\text{eff}} \phi_m) = 0 \quad (12)$$

where $D_{O_{2-m}}$ is oxygen diffusion coefficient in the Nafion phase, $c_{O_{2-m}}$ and ϕ_m are the dissolved oxygen concentration and protonic phase potential in the Nafion phase, respectively, and κ^{eff} is the effective proton conductivity in the Nafion phase of an ordered nanostructured CCL, defined as

$$\kappa^{\text{eff}} = \varepsilon_m \kappa \quad (13)$$

where ε_m is the volume fraction of Nafion in an ordered nanostructured CCL and κ is the intrinsic proton conductivity of Nafion.

The oxygen diffusion coefficient in the Nafion phase ($D_{O_{2-m}}$) is estimated as [50]:

$$D_{O_{2-m}} = 3.1 \times 10^{-3} \exp\left(-\frac{2768}{T}\right) \quad (14)$$

where T is in K, and $D_{O_{2-m}}$ is in $\text{cm}^2 \text{ s}^{-1}$.

The cathode potential in the model is defined as

$$\text{Cathode potential} = E_r - \eta_{act} - \eta_{ohm} \quad (15)$$

where E_r is the thermodynamic reversible cell potential, η_{act} is the potential loss due to resistance to electrochemical reaction and mass transfer limitations in the CCL, also referred here as cathode activation overpotential, and η_{ohm} is the potential loss due to proton transport in the CCL, also referred to as cathode ohmic overpotential, which can be found using the Ohm's law. The thermodynamic reversible cell potential (E_r) as a function of operating temperature, pressure and reactant concentrations, can be expressed as [50]:

$$E_r = 1.23 - 0.9 \times 10^{-3}(T - 298) + \frac{RT}{4F} \ln(p_{H_2}^2 p_{O_2}) \quad (16)$$

where p_{H_2} and p_{O_2} are the partial pressures (in atm) of hydrogen and oxygen, respectively.

The dissolved oxygen concentration at the interface between the pore phase and the Nafion phase is related to the gaseous oxygen concentration using the Henry's law, expressed as [50,51]:

$$c_{O_{2-m}}|_{r_b} = \frac{1}{H_{O_{2-m}}} c_{O_{2-g}}|_{r_b} \quad (17)$$

where $c_{O_{2-g}}|_{r_b}$ is the gaseous oxygen concentration at the interface of the Nafion phase and the pore phase and $H_{O_{2-m}}$ is the Henry's constant for oxygen dissolution in the Nafion film, which is calculated using the empirical correlation [52,53]:

$$H_{O_{2-m}} = 0.1013 \exp\left(14.1 - \frac{666}{T}\right) \quad (18)$$

where the temperature T is in K, and $H_{O_{2-m}}$ is in $\text{Pa m}^3 \text{ mole}^{-1}$ or J mole^{-1} .

Similarly, at the interface between the Nafion phase and CNT phase of an ordered nanostructured CCL, ORR takes place and its rate expression is given by the Butler–Volmer equation, expressed as

$$R_c = A_{i,j} \omega_{0,ref} \left(\frac{c_{O_{2-m}}|_{r_{CNT}}}{c_{O_{2,ref}}} \right)^{\gamma} \left\{ \exp\left(\frac{\alpha_c F \eta_{act}}{RT}\right) - \exp\left(-\frac{\alpha_a F \eta_{act}}{RT}\right) \right\} \quad (19)$$

Table 1
Governing equations.

Multi-component mixture transport	$\nabla \cdot \vec{N}_i = 0$
	$-c \nabla x_i = \sum_{j=1,i}^n \frac{1}{\psi_{ij}^{eff}} (x_j \vec{N}_i - x_i \vec{N}_j)$
Dissolved oxygen transport	$\nabla \cdot (D_{O_{2-m}} c_{O_{2-m}}) = 0$
Proton transport	$\nabla \cdot (\kappa^{eff} \phi_m) = 0$

where A_v is the reactive surface area density, $J_{0,ref}$ is the reference exchange current density measured at a reference oxygen concentration ($c_{O_{2,ref}}$), $c_{O_{2-m}}|_{r_{CNT}}$ is the dissolved oxygen concentration at the reaction interface, γ is the reaction order, which is usually equal to one, α_c and α_a are the cathodic and anodic transfer coefficients, respectively, and η_{act} is the cathode activation overpotential, defined as

$$\eta_{act} = \phi_s - \phi_m \quad (20)$$

where ϕ_s is the electronic phase potential in the electron-conducting phase (CNT) of an ordered nanostructured CCL.

The reactive surface area density is given by [54]:

$$A_v = \frac{m_{Pt} A_s}{L_{CNT}} \quad (21)$$

where m_{Pt} is the catalyst loading per unit area of the cathode, A_s is the catalyst surface area per unit mass of the catalyst, and L_{CNT} is the length of the CNT or thickness of the CCL in an ordered nanostructured CCL.

The reference exchange current density ($J_{0,ref}$) for ORR is obtained using an empirical correlation based on the experimental data of Parthasarathy et al. [55], expressed as

$$\log(J_{0,ref}) = 3.507 - \frac{4001}{T} \quad (22)$$

where $J_{0,ref}$ is in $A\ cm^{-2}$ and T is in K.

Finally, the governing equations in an ordered nanostructured CCL are summarized in Table 1.

3. Boundary conditions

The boundary conditions required to complete the model formulation can be classified into external and internal boundary conditions. External boundary conditions are applied at the external boundaries of the computational domain shown in Fig. 3. Whereas, internal boundary conditions are applied at the interfaces between the pore phase and the Nafion phase,

Table 2
Boundary conditions.

Locations	Boundary conditions
$x=0$	$w_i = \text{specified}$ $\frac{\partial c_{O_{2-m}}}{\partial x} = 0$ $\frac{\partial \phi_m}{\partial x} = 0$ $\frac{\partial w_i}{\partial x} = 0$
$x=L_{CNT}$	$\frac{\partial c_{O_{2-m}}}{\partial x} = 0$ $\eta_0 = \text{specified}$ $\vec{N}_i \cdot \vec{n} = 0$ $\vec{N}_{O_{2-m}} \cdot \vec{n} = 0$ $\vec{J}_m \cdot \vec{n} = 0$
y and z external boundaries	$\vec{N}_i \cdot \vec{n} = 0$ $\vec{N}_{O_{2-m}} \cdot \vec{n} = 0$ $\vec{J}_m \cdot \vec{n} = 0$
r_{CNT}	$N_{O_{2-m}} = -\frac{R_c L_{CNT}}{4F}$ $J_m = -R_c L_{CNT}$
r_b	$c_{O_{2-m}} = \frac{c_{O_{2-g}}}{H_{O_{2-m}}}$ $J_m = 0$

and between the CNT phase and the Nafion phase of the computational domain, also referred to as the interfacial boundary conditions.

Since the computational domain considered is a symmetric portion of an ordered nanostructured CCL, symmetric boundary conditions are applicable at the external boundaries of y and z axes. In contrary, at the external boundary interfacing with GDL (indicated by $x=0$ in Fig. 3), mass fractions of multi-component mixture species are specified, protonic current density and dissolved oxygen flux are set as zero. Similarly, at the external boundary interfacing with the membrane (indicated by $x=L_{CNT}$ in Fig. 3), cathode overpotential is specified, diffusional flux for multi-component mixture species and dissolved oxygen flux are set as zero.

The locations at which internal boundary conditions are required in the model formulation are illustrated as r_{CNT} and r_b . At the interface between the CNT phase and Nafion phase (r_{CNT}), ORR takes place, also referred to as the reaction boundary, reaction boundary conditions are applied for the dissolved oxygen and proton transport. On the other hand, at the interface between the pore phase and Nafion phase (r_b), Henry's law is applied to relate the dissolved oxygen concentration with the gaseous oxygen concentration in the pore phase, and protonic current density is set as zero. The mathematical form of boundary conditions applied is tabulated in Table 2.

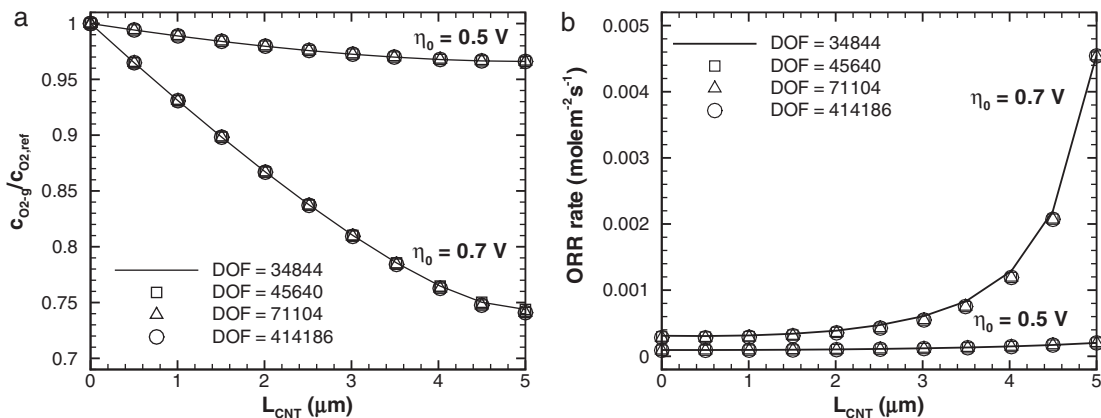


Fig. 4. Distributions of normalized gaseous oxygen concentration (a) and ORR rate (b) along the length of CNT in an ordered nanostructured CCL at different specified overpotentials.

Table 3
Parameters used for model validation.

Operating temperature, T	343.0 K
Pressure, p	2.0 atm
Oxygen concentration at the GDL/CCL interface, c_0	70.13 mole m^{-3} (estimated)
Reference oxygen concentration, $c_{O_2,ref}$	1.0 mole m^{-3}
Radius of CNT, r_{CNT}	25 nm
Thickness of the Nafion film, t_{Nafion}	5 nm
Distance between two CNTs, d_{CNTs}	50 nm (assumed)
Length of CNT, L_{CNT}	5 μm
Intrinsic proton conductivity of Nafion, κ	7.0 S m^{-1} [57]
Pt loading, m_{Pt}	0.2 mg cm^{-2}
Specific surface area of Pt particles, A_s	100 $m^2 g^{-1}$
Membrane thickness, t_m	164 μm [56]
Fixed charge concentration in the membrane, c_{H^+}	1200 mole m^{-3} [56]
Hydraulic permeability of the membrane, K_p	$1.8 \times 10^{-18} m^2$ [56]
Electrokinetic permeability of the membrane, K_E	$7.18 \times 10^{-20} m^2$ [56]

Source: Li et al. [18].

4. Numerical implementation

The governing equations along with boundary conditions presented in the above section are solved using a commercial package, commonly known as COMSOL Multiphysics™. The package uses finite element method to solve the governing partial differential equations (PDEs) over a defined geometry. The computational domain is discretized into tetrahedral mesh and Lagrangian-quadratic elements of second order are used. Since the governing PDEs form a set of non-linear equations, a non-linear solver is used to obtain the solution. The solution is considered to be a converged when the relative tolerance reaches below 10^{-6} .

Additionally, a grid sensitivity test has been conducted to ensure grid independent solution. It also ensures the adequacy of mesh elements used in the 3D computational domain. Different level of mesh sizes are considered ranging approximately from 35,000 to 0.4 million degrees of freedom (DOF). The grid sensitivity results are shown in Fig. 4, which illustrate normalized gaseous oxygen concentration and ORR rate along the length of CNT at different specified overpotentials. It can be observed from the figure that all the grid sizes exhibit almost identical results, indicating grid independent solution. However, for better accuracy, the results presented in the subsequent figures are for higher grid level (DOF = 71104).

5. Model validation

Model validation is as important as model development. It helps in determining the range of validity and accuracy of the model. However, none of the previous models [41–44] of an ordered nanostructured CCL attempted to validate or compare their predictions with the measured data available in the literature. The parameters used in the validation of the present model are listed in Table 3.

Most of the parameters used in the model validation are obtained from Li et al. [18], who reported the measured cell performance data having an ordered nanostructured CCL. Since the present model predicts an ordered nanostructured CCL performance, to compare with the measured cell performance, the membrane ohmic overpotential is accounted using an expression presented by Baschuk and Li [56]:

$$\eta_m = t_m \left(\frac{(J_m/\kappa) + (FK_p c_{H^+} \Delta p_{a-c} / \kappa \mu_{H_2O} t_m)}{1 + (F^2 K_E c_{H^+}^2 / \kappa \mu_{H_2O})} \right) \quad (23)$$

where t_m is the membrane thickness, K_p is the hydraulic permeability of the membrane, c_{H^+} is the fixed charge concentration in the membrane, Δp_{a-c} is the pressure difference between the anode

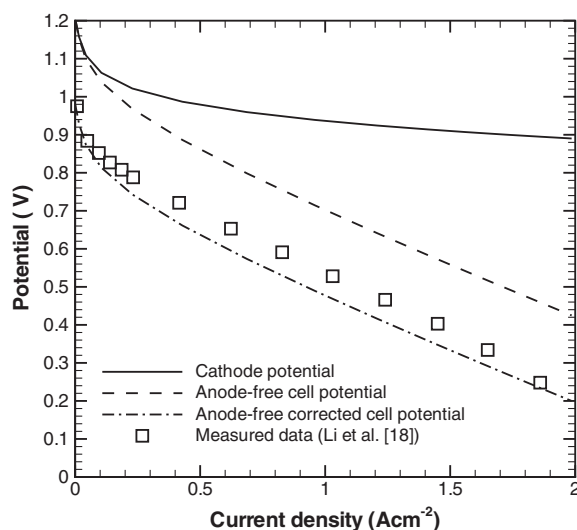


Fig. 5. Comparison between the predicted and measured cell performance having an ordered nanostructured CCL.

and the cathode μ_{H_2O} is the viscosity of liquid water, and K_E is the electrokinetic permeability of the membrane.

Fig. 5 shows the comparison between the predicted and measured cell performance having an ordered nanostructured CCL. The lines represent the model predictions, while the symbol represents the measured cell performance data obtained from Li et al. [18]. The solid line represents the predicted ordered nanostructured CCL performance at 343 K and 2 atm. When the contribution of membrane overpotential is taking into account in addition to the cathode overpotential towards the total cell potential loss, the predicted performance curve is shown by the dashed line, referred to as the 'anode-free cell potential' in Fig. 5. It can be seen that the predicted anode-free cell performance exhibits similar trend as the measured cell performance with a constant difference throughout the current density range, indicating the difference originating from the potential difference between the calculated thermodynamic reversible cell potential and the measured open-circuit cell potential at zero load, also referred to as the mixed electrode potential in the literature [58–60]. It is reported to be in the order of 0.1–0.2 V, and arises due to unavoidable parasitic reactions and fuel crossover through the membrane [53,60]. When the anode-free cell potential is corrected with the mixed electrode potential, the resulting cell performance curve is shown by the dashdot line in Fig. 5, and referred to as the anode-free corrected cell potential. Further, it can be seen that anode-free corrected cell potential is in good agreement with the measured data.

6. Results and discussion

The developed model not only predicts the distributions of various fields in different phases of an ordered nanostructured CCL but also predicts the ordered nanostructured CCL performance at various operating and design conditions. The base case parameters used in the simulation are listed in Table 4.

Fig. 6 shows the distributions of gaseous oxygen concentration in the pore phase of an ordered nanostructured CCL at various applied overpotentials at the membrane interface. The horizontal-axis represents the length of CNT, can also be referred as the thickness of the nanostructured CCL, while the vertical-axis represents the gaseous oxygen concentration (c_{O_2-g}) in the pore phase. The effect of Knudsen diffusion is not considered in the base case simulation. A more detailed examination of the effect Knudsen diffusion with CNT spacing (d_{CNTs}) is presented in the following

Table 4
Base case parameters used in the simulation.

Operating temperature, T	353.0 K
Pressure, p	1.0 atm
Molar diffusion volume of oxygen, ν_{O_2}	$16.6 \times 10^{-6} \text{ m}^3 \text{ mole}^{-1}$ [61]
Molar diffusion volume of water vapor, ν_{H_2O}	$12.7 \times 10^{-6} \text{ m}^3 \text{ mole}^{-1}$ [61]
Molar diffusion volume of nitrogen, ν_{N_2}	$17.9 \times 10^{-6} \text{ m}^3 \text{ mole}^{-1}$ [61]
Mass fraction of oxygen at the GDL/CCL interface, w_{O_2}	0.1447
Mass fraction of water vapor at the GDL/CCL interface, w_{H_2O}	0.3789
Reference oxygen concentration, $c_{O_2,ref}$	$2.637 \text{ mole m}^{-3}$
Cathode transfer coefficient, α_c	0.58
Anode transfer coefficient, α_a	1
Radius of CNT, r_{CNT}	25 nm
Thickness of the Nafion film, t_{Nafion}	10 nm
Distance between two CNTs, d_{CNTs}	50 nm
Length of CNT, L_{CNT}	$5 \mu\text{m}$
Pore volume fraction, ε_g	0.739
Nafion volume fraction, ε_m	0.130
Intrinsic proton conductivity of Nafion, κ	7.0 S m^{-1}
Pt loading, m_{Pt}	0.2 mg cm^{-2}
Specific surface area of Pt particles, A_s	$100 \text{ m}^2 \text{ g}^{-1}$

section. It can be seen that there is negligible variation in the concentration of gaseous oxygen (c_{O_2-g}), as we move along the length of CNT for $\eta_0 = 0.3 \text{ V}$. However, with the increase of applied overpotential at the membrane interface, the gaseous oxygen concentration (c_{O_2-g}) decreases along the length of CNT with a substantial drop at $\eta_0 = 0.7 \text{ V}$. Increasing the applied overpotential (η_0) increases the ORR rate at the reaction boundary along the length of CNT (can be evident from Fig. 7), resulting in the increased consumption of dissolved oxygen, which in turn decreases the concentration of gaseous oxygen (c_{O_2-g}) in the pore phase. Moreover, this is due to multi-component diffusion in the pore phase, wherein the concentration of gaseous oxygen depends on the concentration of other $n - 1$ species. Similarly, the distributions of dissolved oxygen concentration at the reaction boundary along the length of CNT at various applied overpotentials is shown in Fig. 8. The horizontal-axis represents the length of CNT, while the vertical-axis represents the dissolved oxygen concentration (c_{O_2-m}). Again, similar trends can be observed for the dissolved oxygen concentration (c_{O_2-m}) with increasing applied overpotential (η_0) at the membrane interface.

On the other hand, the distributions of dissolved oxygen concentration (c_{O_2-m}) within the Nafion film of an ordered nanostructured

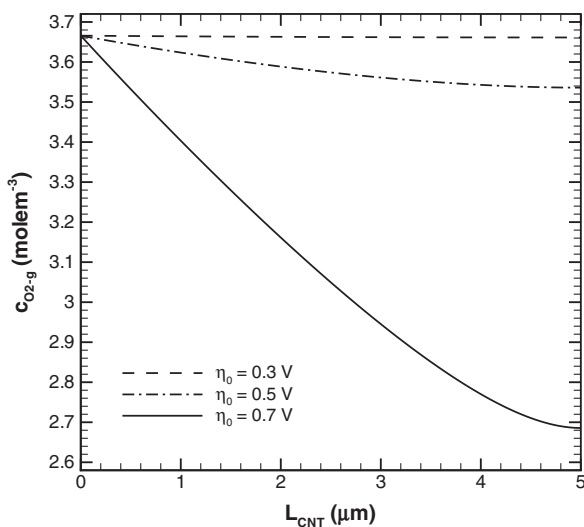


Fig. 6. Distributions of gaseous oxygen concentration along the length of CNT in an ordered nanostructured CCL at different specified overpotentials.

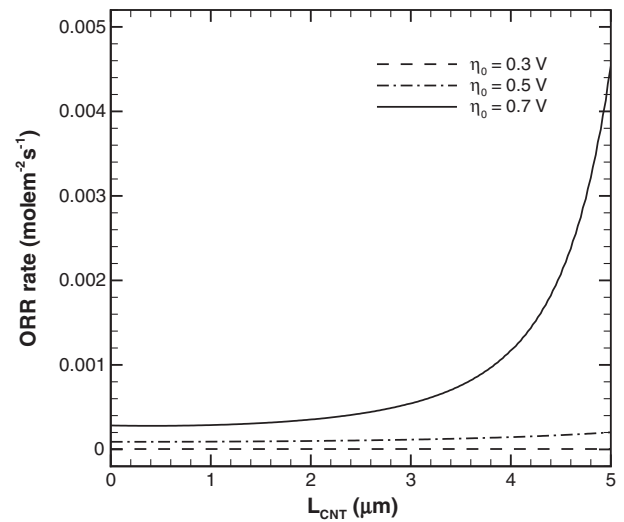


Fig. 7. Distributions of ORR rate at the reaction boundary along the length of CNT in an ordered nanostructured CCL at different specified overpotentials.

CCL at different applied overpotentials is shown in Fig. 9. The horizontal-axis represents the thickness of the Nafion film, while the vertical-axis represents the dissolved oxygen concentration (c_{O_2-m}). It can be seen that the dissolved oxygen concentration (c_{O_2-m}) exhibits linear variation along the thickness of the Nafion film at all the applied overpotentials (η_0). Moreover, it can be seen that the dissolved oxygen concentration decreases as we move from right to the left, indicating the consumption of dissolved oxygen at the reaction boundary (corresponds to $t_{Nafion} = 0$ in Fig. 9). Further, it is worth mentioning that the concentration of dissolved oxygen at the right (corresponds to $t_{Nafion} = 10 \text{ nm}$ in Fig. 9) is governed by the Henry's law, indicating the interface between the Nafion phase and the pore phase.

7. Effect of Knudsen diffusion

Knudsen diffusion becomes important when mean pore diameter in porous media (in other words, mean distance or spacing between two CNTs in an ordered nanostructured CCL) is comparable to the mean free path of the gas molecule. According to Jennings

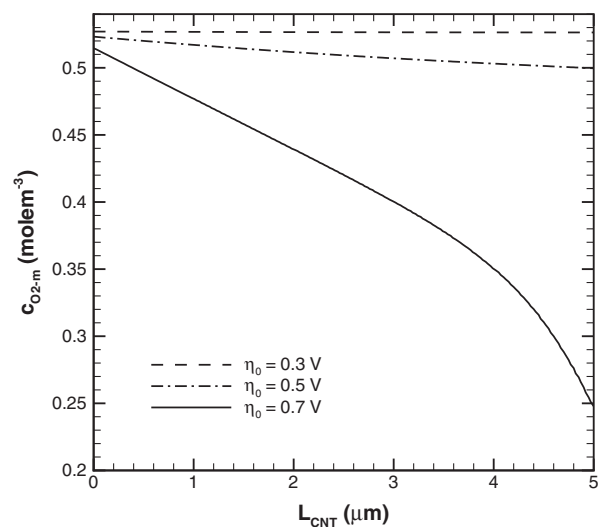


Fig. 8. Distributions of dissolved oxygen concentration at the reaction boundary along the length of CNT in an ordered nanostructured CCL at different specified overpotentials.

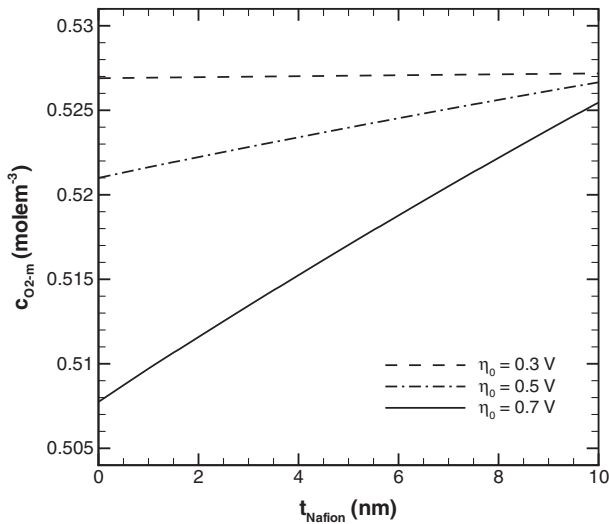


Fig. 9. Distributions of dissolved oxygen concentration within the Nafion film of an ordered nanostructured CCL at different specified overpotentials.

[62] expression, the mean free path of air molecule at 353 K and 1 atm is about 80 nm, which is comparable to the mean distance or spacing between two CNTs (d_{CNTs}) at the base case simulation conditions, indicating the diffusion to be in the transition regime. Fig. 10 shows the effect of Knudsen diffusion on the distribution of gaseous oxygen concentration in the pore phase of an ordered nanostructured CCL at an applied overpotential of 0.7 V using the base case parameters listed in Table 4. Again, the horizontal-axis represents the length of CNT, while the vertical-axis represents the gaseous oxygen concentration (c_{O_2-g}) in the pore phase. Further, the solid line represents the concentration of gaseous oxygen when Knudsen diffusion is not taken into account with the ordinary diffusion; whereas, the dashed line represents the concentration of gaseous oxygen (c_{O_2-g}) when Knudsen diffusion is taken into account with the ordinary diffusion in the pore phase. It can be seen that the difference in the concentration of oxygen between the Knudsen and non-Knudsen diffusion increases as we move along the length of the CNT. However, the average drop in oxygen concentration along the length of CNT between the Knudsen and

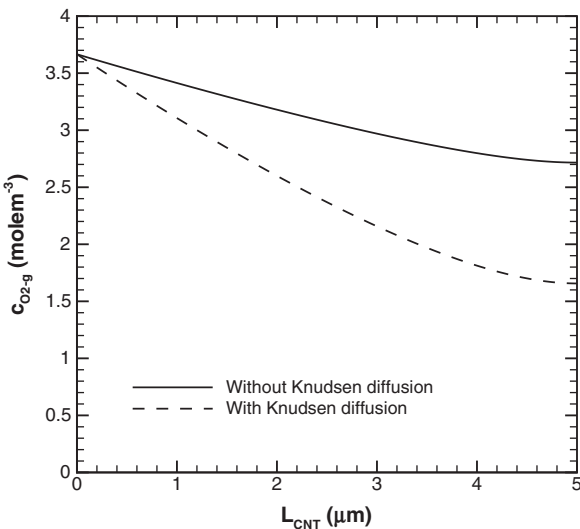


Fig. 10. Effect of Knudsen diffusion on the gaseous oxygen concentration in the pore phase of an ordered nanostructured CCL at $\eta_0 = 0.7$ V using the base case parameters listed in Table 4.

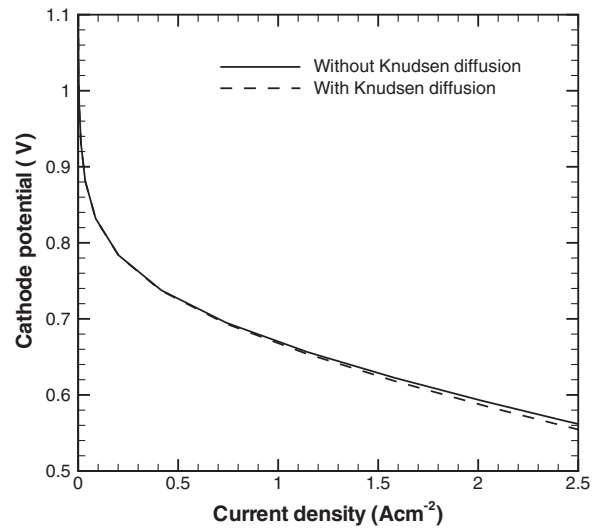


Fig. 11. Effect of Knudsen diffusion on the performance of an ordered nanostructured CCL at the base case conditions listed in Table 4.

non-Knudsen diffusion is of the same order of magnitude, resulting in a negligible effect on the performance of an ordered nanostructured CCL at the base case conditions, which can be evident from Fig. 11. Additionally, the Knudsen diffusion coefficients ($D_{Kn,i}$) of species i , which depends on the distance (spacing) between two CNTs (d_{CNTs}), are of the same order of magnitude as of ordinary diffusion coefficients (D_{ij}) at the base case conditions.

Similarly, the effect of Knudsen diffusion on the performance of an ordered nanostructured CCL at the CNT spacing of 25 nm is shown in Fig. 12. It can be observed that there is an appreciable difference in the performance of an ordered nanostructured CCL between the Knudsen and non-Knudsen diffusion when the CNT spacing is reduced to half ($d_{CNTs} = 25$ nm) of the base case CNT spacing. This is due to the Knudsen diffusion coefficients ($D_{Kn,i}$) of species i , which are an order of magnitude smaller than the ordinary diffusion coefficients (D_{ij}) when the CNT spacing is reduced to half of the base case CNT spacing ($d_{CNTs} = 25$ nm). Moreover, because of straight pores and high porosity in an ordered nanostructured CCL, Knudsen diffusion effect can be assumed negligible above the CNT spacing (d_{CNTs}) of 25 nm. Therefore, the effect of Knudsen diffu-

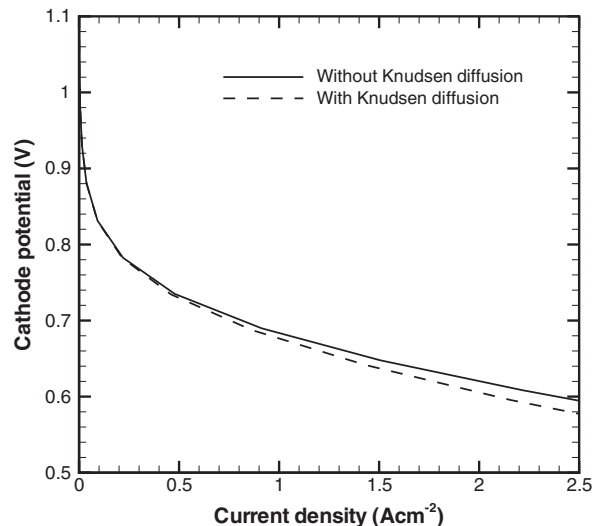


Fig. 12. Effect of Knudsen diffusion on the performance of an ordered nanostructured CCL at $d_{CNTs} = 25$ nm.

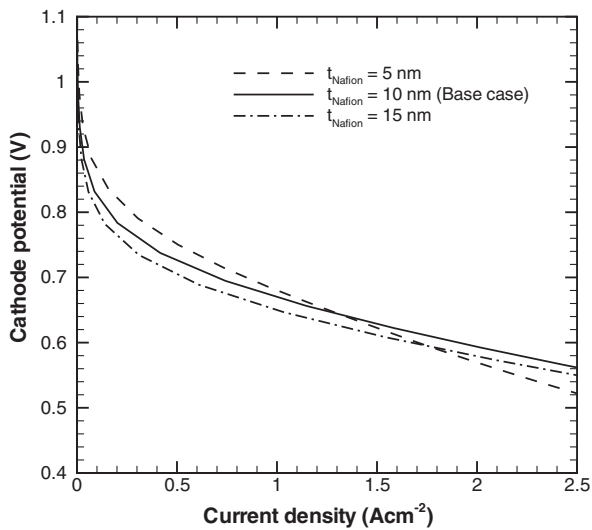


Fig. 13. Effect of Nafion thickness (t_{Nafion}) on the performance of an ordered nanostructured CCL.

sion is not considered for the base case CNT spacing ($d_{\text{CNTs}} = 50 \text{ nm}$), implying the simulation results presented in the previous and subsequent sections consider only the ordinary diffusion in the pore phase of an ordered nanostructured CCL.

8. Effect of Nafion thickness (t_{Nafion})

Fig. 13 shows the effect of Nafion film thickness (t_{Nafion}) on the performance of an ordered nanostructured CCL. All the operating and design parameters are kept same as the base case parameters listed in Table 4. However, it is worthwhile to mention that changing a design parameter changes the overall volume of the computational domain, which in turn change the volume fractions of pore phase and Nafion phase of an ordered nanostructured CCL. It can be seen that the performance of an ordered nanostructured CCL exhibits mixed trends with increasing the thickness of Nafion film. The performance of an ordered nanostructured CCL decreases with the increase of Nafion film thickness for current densities up to 1 A cm^{-2} . However, beyond the current density of 1 A cm^{-2} , the ordered nanostructured CCL with thinnest Nafion film shows poorer performance. This is due to trade-off between the dissolved oxygen transport and the proton transport with increasing Nafion film thickness, and the variations of activation overpotential and ohmic overpotential with current density at different Nafion film

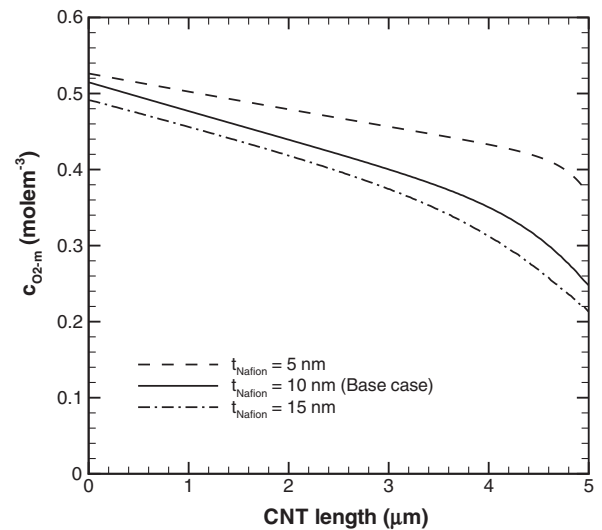


Fig. 15. Distributions of dissolved oxygen concentration at the reaction boundary along the length of CNT in an ordered nanostructured CCL at different Nafion thicknesses at $\eta_0 = 0.7 \text{ V}$.

thicknesses in an ordered nanostructured CCL is shown in Fig. 14. It can be observed from Fig. 14 that increasing the Nafion film thickness in an ordered nanostructured CCL increases the cathode activation overpotential; on the other hand, the cathode ohmic overpotential decreases with the increases of Nafion film thickness. This is due to increase in resistance to the diffusion of dissolved oxygen to the reaction boundary with increasing Nafion film thickness, resulting in the reduction of dissolved oxygen concentration at the reaction boundary, as can be evident from Fig. 15. However, decreasing the Nafion film thickness results in the reduction of Nafion volume fraction in an ordered nanostructured CCL, which in turn reduces the effective conductivity of proton in the Nafion film, and thereby increases the ohmic overpotential with decreasing Nafion film thickness. The optimal thickness for the Nafion film in an ordered nanostructured CCL is found to be 10 nm from the present simulation, which is in accordance with the Nafion film thickness reported by Middelmann [3].

9. Effect of CNT length (L_{CNT})

The effect of different CNT lengths on the performance of an ordered nanostructured CCL is shown in Fig. 16. The other operating and design parameters are kept similar to the base case

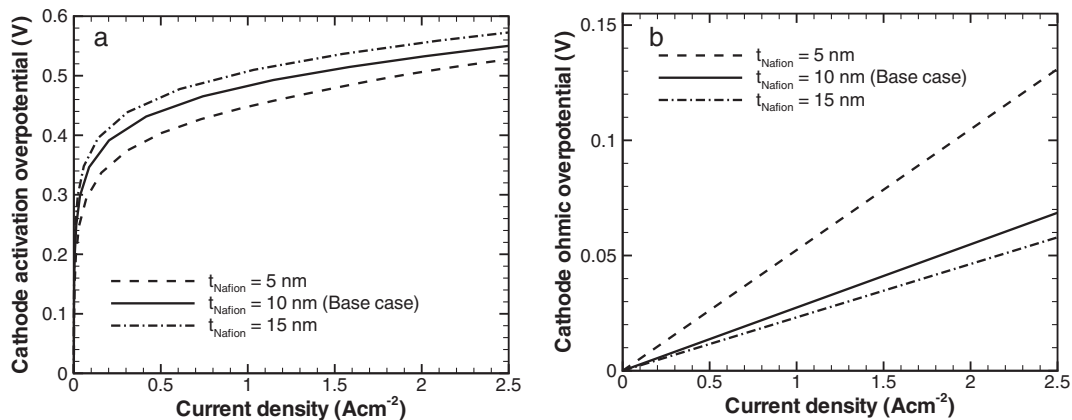


Fig. 14. Variations of activation overpotential (a) and ohmic overpotential (b) in an ordered nanostructured CCL with current density at different Nafion film thicknesses.

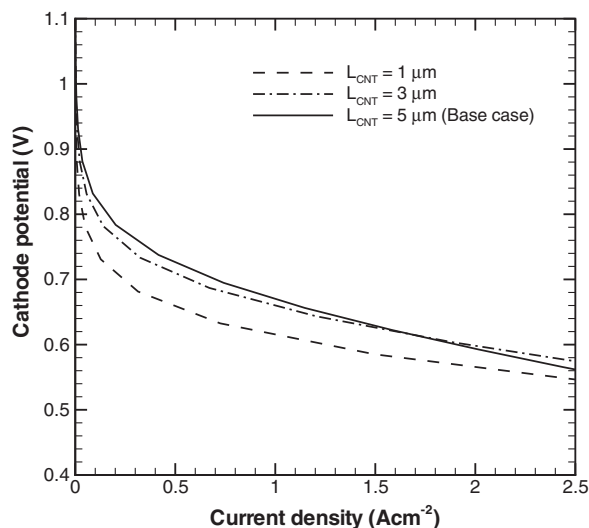


Fig. 16. Effect of CNT length (L_{CNT}) on the performance of an ordered nanostructured CCL.

parameters listed in Table 4. Again, the ordered nanostructured CCL performance exhibits mixed trends with increasing CNT lengths. It can be observed that increasing the CNT length increases the performance of an ordered nanostructured CCL below the current density of 1.5 A cm^{-2} . However, beyond the current density of 2 A cm^{-2} , the ordered nanostructured CCL with $3 \mu\text{m}$ CNT length exhibits better performance than the base case CNT length ($5 \mu\text{m}$). This is again due to trade-off between the activation overpotential and the ohmic overpotential of an ordered nanostructured CCL with increasing CNT thickness, and the variations of activation and ohmic overpotentials with current density at different CNT lengths is shown in Fig. 17. It can be seen from Fig. 17 that increasing CNT length in an ordered nanostructured CCL decreases the activation overpotential and increases the ohmic overpotential. This can be attributed to more reaction sites with increasing CNT length, resulting in the reduction of activation overpotential; in contrary, increasing the CNT length increases the transport distance for protons, resulting in increasing ohmic overpotential with increasing CNT length. The optimal CNT length for an ordered nanostructured CCL is found to be $3 \mu\text{m}$ from the range of CNT lengths considered in the present simulation.

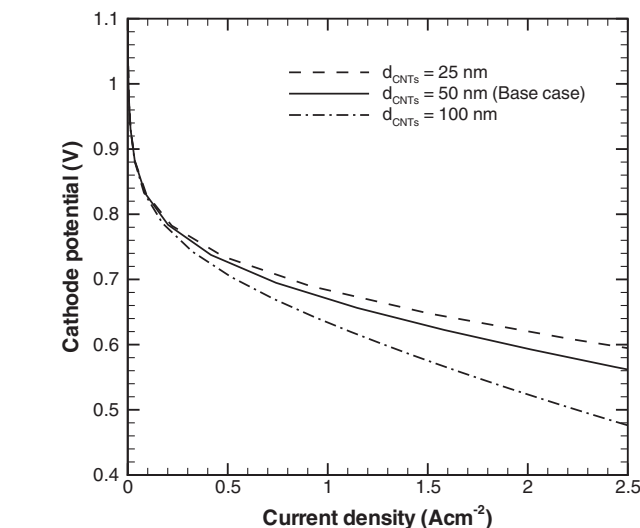
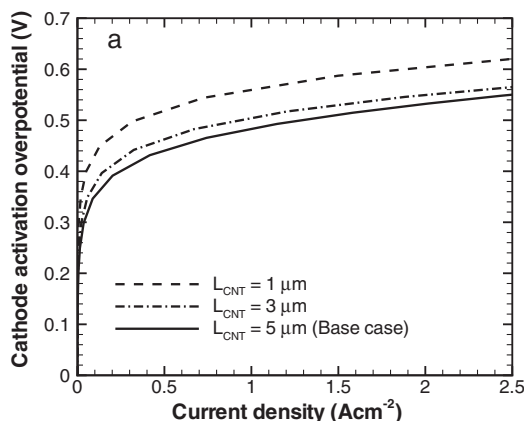


Fig. 18. Effect of CNT spacing (d_{CNT}) on the performance of an ordered nanostructured CCL.

10. Effect of CNT spacing (d_{CNTs})

The effect of various CNT spacings on the performance of an ordered nanostructured CCL is shown in Fig. 18. The other operating and design parameters are kept similar to the base case parameters listed in Table 4. Moreover, Knudsen diffusion is not considered here even with the CNT spacing of 25 nm . It can be seen that increasing the CNT spacing results in a considerable drop in performance of an ordered nanostructured CCL. Increasing the CNT spacing in an ordered nanostructured CCL decreases the number of CNTs being accommodated in a fixed volume. Consequently, the volume fraction of Nafion decreases with increasing CNT spacing, resulting in the increase of resistance to proton transport. As a result, cathode ohmic overpotential increases significantly with increasing CNT spacing, which can be evident from Fig. 19. Moreover, it can be seen from Fig. 19 that the CNT spacing has a negligible effect on the cathode activation overpotential. This is due to insignificant effect of porosity in an ordered nanostructured CCL, which increases with the increase of CNT spacing. Further, the CNT spacing of 50 nm is found to be optimum for the range of CNT spacings considered in the present simulation.

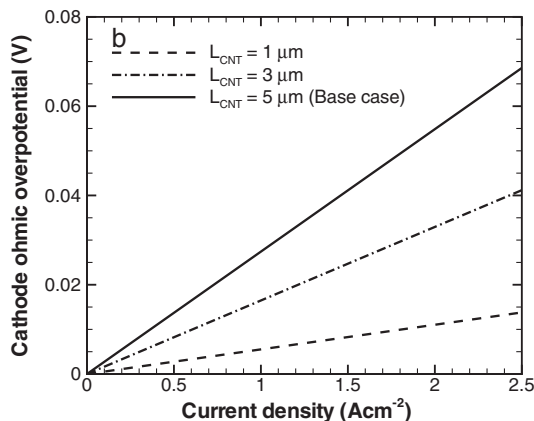


Fig. 17. Variations of activation overpotential (a) and ohmic overpotential (b) in an ordered nanostructured CCL with current density at different CNT lengths.

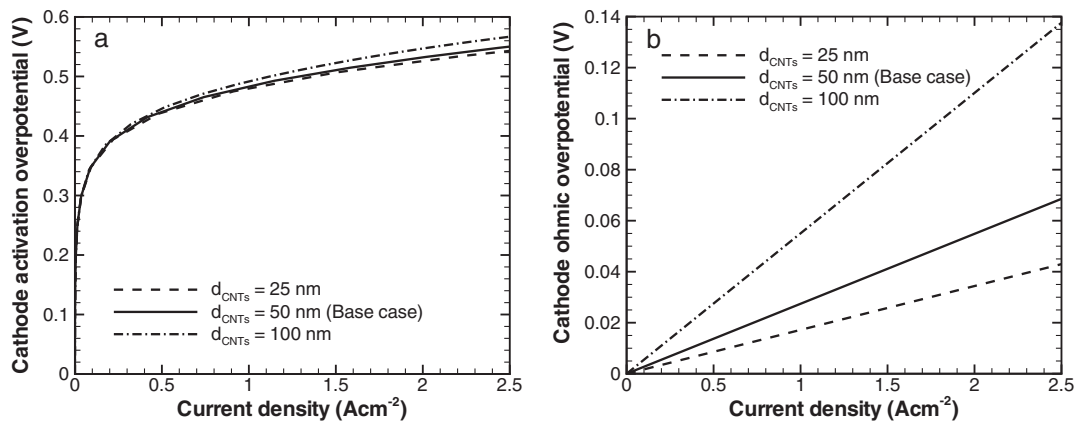


Fig. 19. Variations of activation overpotential (a) and ohmic overpotential (b) in an ordered nanostructured CCL with current density at different CNT spacings.

11. Conclusions

A 3D mathematical model of an ordered nanostructured CCL has been developed for PEM fuel cells. The model includes all the relevant processes in different phases of an ordered nanostructured CCL. Also, the model takes into account the effect of Knudsen diffusion. The model predicts not only the performance of an ordered nanostructured CCL at various operating and design conditions but also predicts the distributions of various fields in different phases of an ordered nanostructured CCL. The predicted nanostructured CCL performance with estimated membrane overpotential is validated with measured data found in the literature, and obtained a good agreement between the model prediction and measured result. Additionally, a parametric study is also performed to examine the effect of key design parameters on the performance of an ordered nanostructured CCL. In the absence of liquid water, it is found that gaseous oxygen diffusion in the pore phase is not the limiting factor for the performance of nanostructured CCL, owing to its parallel gas pores and high porosity. However, diffusion of dissolved oxygen through the Nafion film has a significant effect on the performance of nanostructured CCL. Further, it is found that the effect Knudsen diffusion is negligible on the performance of an ordered nanostructured CCL above the CNT spacing (d_{CNTs}) of 25 nm. Furthermore, the optimal thickness for the Nafion film in an ordered nanostructured CCL is found to be 10 nm, consistent with the Nafion film thickness reported by Middelmann [3].

References

- [1] J. Xie, D.L. Wood, D.M. Wayne, T.A. Zawodzinski, P. Atanassov, R.L. Borup, J. Electrochem. Soc. 152 (2005) A104–A113.
- [2] R. Borup, J. Meyers, B. Pivovar, Y.S. Kim, R. Mukundan, N. Garland, D. Myers, M. Wilson, F. Garzon, D. Wood, P. Zelenay, K. More, K. Stroh, T. Zawodzinski, J. Boncella, J.E. McGrath, M. Inaba, K. Miyatake, M. Hori, K. Ota, Z. Ogumi, S. Miyata, A. Nishikata, Z. Siroma, Y. Uchimoto, K. Yasuda, K.-I. Kimijima, N. Iwashita, Chem. Rev. 107 (2007) 3904–3951.
- [3] E. Middelmann, Fuel Cells Bull. 11 (2002) 9–12.
- [4] M. Waje, W. Li, Z. Chen, Y. Yan, ECS Trans. 3 (1) (2006) 677–683.
- [5] S.D. Knights, K.M. Colbow, J. St-Pierre, D.P. Wilkinson, J. Power Sources 127 (2004) 127–134.
- [6] D. Stevens, M. Hicks, G. Haugen, J. Dahn, J. Electrochem. Soc. 152 (12) (2005) A2309.
- [7] R.M. Darling, J.P. Meyers, J. Electrochem. Soc. 150 (11) (2003) A1523–A1527.
- [8] R.M. Darling, J.P. Meyers, J. Electrochem. Soc. 152 (1) (2005) A242–A247.
- [9] M.K. Debe, A.K. Schmoedel, G.D. Vernstrom, R. Atanasoski, J. Power Sources 161 (2006) 1002–1011.
- [10] T.R. Ralph, M.P. Hogarth, Platinum Met. Rev. 46 (2002) 3–14.
- [11] K.H. Kangasniemi, D.A. Condit, T.D. Jarvi, J. Electrochem. Soc. 151 (2004) E125–E132.
- [12] J.G. Liu, Z.H. Zhou, X.X. Zhao, Q. Xin, G.Q. Sun, B.L. Yi, Chem. Phys. 6 (2004) 134–137.
- [13] Y. Shao, G. Yin, Y. Gao, J. Power Sources 171 (2007) 558–566.
- [14] S. Litster, G. McLean, J. Power Sources 130 (2004) 61.
- [15] G.S. Kumar, M. Raja, S. Parthasarathy, Electrochim. Acta 40 (1995) 285–290.
- [16] A.M. Kannan, V.P. Veedu, L. Munukutla, M.N. Ghasemi-Nejhad, Electrochem. Solid-State Lett. 10 (3) (2007) B47–B50.
- [17] T. Hatanaka, H. Nakanishi, S. Matsumoto, Y. Morimoto, ECS Trans. 3 (1) (2006) 277–284.
- [18] W. Li, X. Wang, Z. Chen, M. Waje, Y. Yan, Langmuir 21 (2005) 9386–9389.
- [19] M. Waje, W. Li, Z. Chen, Y. Yan, ECS Trans. 3 (1) (2006) 285–294.
- [20] A.J. Steinbach, K. Noda, M.K. Debe, ECS Trans. 3 (1) (2006) 835–853.
- [21] N. Job, S. Berthon-Fabry, M. Chatenet, J. Marie, M. Brigaudet, J.-P. Pirard, Top. Catal. 52 (2009) 2117–2122.
- [22] M. Michel, A. Taylor, R. Sekol, P. Podsiadlo, P. Ho, N. Kotov, L. Thompson, Adv. Mater. 19 (2007) 3859–3864.
- [23] M. Gangeri, G. Centi, A. La Malfa, S. Perathoner, R. Vieira, C. Pham-Huu, M.J. Ledoux, Catal. Today 102–103 (2005) 50–57.
- [24] Z.W. Chen, W.Z. Li, M. Waje, Y. Yan, Angew. Chem. Int. Ed. 46 (2007) 4060–4063.
- [25] X. Wang, M. Waje, Y. Yan, Electrochem. Solid-State Lett. 8 (2005) A42–A44.
- [26] C. Wang, M. Waje, X. Wang, J.M. Tang, R.C. Haddon, Y. Yan, Nano Lett. 4 (2004) 345–348.
- [27] X. Wang, W. Li, M. Waje, Y. Yan, J. Power Sources 158 (2006) 154–159.
- [28] M.S. Saha, R. Li, X. Sun, J. Power Sources 177 (2008) 314–322.
- [29] M.S. Saha, R. Li, M. Cai, X. Sun, J. Power Sources 185 (2008) 1079–1085.
- [30] M.S. Saha, M.N. Banis, Y. Zhang, R. Li, X. Sun, M. Cai, F.T. Wagner, J. Power Sources 192 (2009) 330–335.
- [31] M.S. Saha, A. Kundu, J. Power Sources 195 (2010) 6255–6261.
- [32] Y. Bing, H. Liu, L. Zhang, D. Ghosh, J. Zhang, Chem. Soc. Rev. 39 (2010) 2184–2202.
- [33] R.S. Ruoff, D.C. Lorents, Carbon 33 (1995) 925–930.
- [34] M. Yu, O. Lourie, M.J. Dyer, K. Moloni, T.F. Kelly, R.S. Ruoff, Science 287 (2000) 637–640.
- [35] R.H. Baughman, A.A. Zakhidov, W.A. de Heer, Science 297 (2002) 787–793.
- [36] C. Burda, X.B. Chen, R. Narayanan, M.A. El-Sayed, Chem. Rev. 105 (2005) 1025–1102.
- [37] P.M. Ajayan, O.Z. Zhou, Top. Appl. Phys. 80 (2001) 391–425.
- [38] X. Li, H. Zhou, P. Yu, L. Su, T. Ohsaka, L. Mao, Electrochem. Commun. 10 (2008) 851–854.
- [39] S. Frank, P. Poncharal, Z. Wang, W. de Heer, Science 280 (1998) 1744–1746.
- [40] W. Liang, M. Bockrath, D. Bozovic, J. Hafner, M. Tinkham, H. Park, Nature 411 (2001) 665–669.
- [41] C.Y. Du, X.Q. Cheng, T. Yang, G.P. Yin, P.F. Shi, Electrochem. Commun. 7 (2005) 1411–1416.
- [42] C.Y. Du, T. Yang, P.F. Shi, G.P. Yin, X.Q. Cheng, Electrochim. Acta 51 (2006) 4934–4941.
- [43] M. Chisaka, H. Daiguji, Electrochem. Commun. 8 (2006) 1304–1308.
- [44] S.M. Rao, Y. Xing, J. Power Sources 185 (2008) 1094–1100.
- [45] M.M. Hussain, X. Li, I. Dincer, Int. J. Energy Res. 29 (2005) 1083–1101.
- [46] E.L. Cussler, Diffusion-Mass Transfer in Fluid Systems, Cambridge University Press, New York, 1997.
- [47] S. Biloe, S. Mauran, Carbon 41 (2003) 525–537.
- [48] C.Y. Wang, Chem. Rev. 104 (2004) 4727–4766.
- [49] J.A. Wesselingh, R. Krishna, Mass Transfer in Multicomponent Mixtures, Delft University Press, 2000.
- [50] D.M. Bernadi, M.W. Verbrugge, AIChE 37 (1991) 1151–1163.
- [51] D.M. Bernadi, M.W. Verbrugge, J. Electrochem. Soc. 139 (1992) 2477–2491.
- [52] Z. Ogumi, Z. Takehara, S. Yoshizawa, J. Electrochem. Soc. 131 (1984) 769–773.
- [53] X. Li, Principles of Fuel Cells, Taylor and Francis, New York, 2006.
- [54] C. Marr, X. Li, J. Power Sources 77 (1999) 17–27.
- [55] A. Parthasarathy, S. Srinivasan, J. Appleby, J. Electrochem. Soc. 139 (1992) 2530–2537.
- [56] J.J. Baschuk, X. Li, J. Power Sources 86 (2000) 181–196.
- [57] Y. Sone, P. Ekdunge, D. Simonsson, J. Electrochem. Soc. 143 (1996) 1254–1259.

- [58] M. Eikerling, A.A. Kornyshev, A.M. Kuznetsov, J. Ulstrup, S. Walbran, J. Phys. Chem. B 105 (2001) 3646–3662.
- [59] A.F. Gulla, M.S. Saha, R.J. Allen, S. Mukherjee, J. Electrochem. Soc. 153 (2006) A366–A371.
- [60] P.K. Das, X. Li, Z.-S. Liu, J. Electroanal. Chem. 604 (2007) 72–90.
- [61] R. Perry, D. Green, Perry's Chemical Engineering Handbook, Seventh ed., McGraw-Hill, 1997.
- [62] S.G. Jennings, J. Aerosol Sci. 19 (1988) 159–166.